Constitutive Relationship Development, Modeling and Measurement of Heat Stressing of Micro-SMD Assembly with Sn3.9Ag0.6Cu SAC Alloy

Qiang Xiao[1], William D. Armstrong[1]
James M. Pitarresi[2], Satish C. Chaparala[2], Brian D. Rogeman[2], Bahgat G. Sammakia[2]
Luu Nguyen[3]

[1] Dept. 3295, Mechanical Engineering
University of Wyoming
Laramie, WY 82071, Tel. 307-766-2959
wda@uwyo.edu

[2]Department of Mechanical Engineering
State University of New York, Binghamton, NY, 13902-6000

[3]National Semiconductor Corporation
Santa Clara, CA 95052

ABSTRACT

The Creep and microstructural changes during creep behaviors of bulk and thin cast forms of Sn3.9Ag0.6Cu were compared. The processing parameters of the thin cast material was selected to result in a very fine microstructure analogous to what occurs in very small size solder electronic interconnections. We found that the thin cast material was less creep-resistant than the bulk material. A comparison of Ag element maps between as crept bulk and thin cast material showed that the relevant climb process occurs in a very different environment in the bulk material as compared to the thin cast material. In the bulk material the relevant climb process occurs within a finely dispersed IMC eutectic which covers broad areas within the material. In the thin cast material the relevant climb process occurs primarily in the beta-Sn grains which continuously surround isolated, coarse IMC particles. This resulted in the activation energy of the bulk material being larger than that for the thin cast material. Finally, it is important to note that the strength deficiency of the thin cast material was persistent, once the material is cast in thin cast form it will remain weak in comparison to the bulk material. Therefore, using data obtained from bulk material samples for the construction of thermo-mechanical models of very small scale solder interconnections is likely to result in significant, intrinsic errors.

Second, the thermal-mechanical response of electronic packages was simulated using the commercial finite element code ANSYS coupled with the Garofalo model to represent the solder constitutive creep response. The measured properties for bulk and thin-cast Sn3.9Ag0.6Cu SAC alloy were used in the FE modeling. A 36 I/O micro-surface mount device (SMD) package was used as a test vehicle in this work. Moiré Interferometry was used to measure the horizontal displacements in the solder joints as a result of cooling the package from 100°C to room temperature. Modeling results were found to have good agreement with moiré measurements on the actual SAC packages.

The bulk properties produced a better correlation with the measurement of the horizontal displacement in the solder joints than the thin-cast properties. However, the assemblies that were tested used the Sn3.8Ag0.6Cu alloy rather than the Sn3.9Ag0.6Cu alloy. It is not known if this difference is significant to the thermo-mechanical response.

KEYWORDS

Lead-free solder, creep, constitutive model micro-structural changes, Finite element model.

INTRODUCTION

Lead-free solder has seen increasing use in interconnection systems for electronic packages due to legislative and marketing pressures. The NEMI, Sn3.9Ag0.6Cu alloy or a close variation, appears to be a leading candidate for broad commercial use. Understanding creep behavior and mechanisms is fundamental to the design of reliable electronic joints since thermal creep fatigue is a primary mechanism of failure of solder joints. Recently, there have been a number of publications that describe new creep constitutive models for near-ternary eutectic SnAgCu alloy. Dutta et al. [1]-[2] developed a microstructurally adaptive creep model, which accounts for the effects of microstructural changes due to aging on the creep response of solder joints, and is capable of adjusting itself as solder joint

microstructures evolve during service. Song et al. [3]-[4] and Hua [5] discovered that the stress exponent has significantly different values between the low and high stress regime. The observation of increasing stress exponent with increasing stress level has led to the general use of the nonlinear Garofalo hyperbolic sine steady state creep model [6]. Lau et al.[7] used compression creep data from 95.5Sn-3.9Ag-0.6Cu bulk solder specimens to identify the parameters of the Garofalo hyperbolic sine function model for use in an accelerated reliability model. Pang et al.[8] and Schubert et al. [9] successfully modeled the steady state tensile creep behavior of bulk 95.Sn-3.8Ag-0.7Cu with the Garofalo hyperbolic sine function, while Zhang et al. [10] successfully used the Garofalo hyperbolic sine function for steady state creep of bulk Sn3.9Ag0.6Cu in shear. Wiese et al. [11] identified different low and high stress mechanisms for steady state creep deformation and used a double power law model to represent creep data on bulk, PCB samples, and Flip Chip solder joint samples of Sn4.0Ag0.5Cu solder.

The above studies have made significant progress in characterizing the steady state creep behavior of SnAgCu solders, however much work still remains to be done. Most importantly, the effects of strong reductions in sample size on the development of microstructure and consequent changes in creep behavior are not well known. This issue is one of increasing importance as the size of electronic solder connections become ever smaller. This paper will compare experimental data between bulk scale [12]-[13] and thin cast samples. The thin cast samples are designed to duplicate the rapid heterogeneous nucleation and small total latent heat characteristics of very small solder balls. Our results show that bulk and thin cast samples exhibit significant differences in creep performance, and therefore we may expect decreased performance from small scale SnAgCu lead-free solder balls under elevated temperature service in an electronic package.

EXPERIMENTAL PROCEDURE

In this study two forms of test sample were investigated, both forms of test sample having the same commercially available NEMI Sn3.9Ag0.6Cu nominal composition (composition given in mass %). In one case, samples were cast with a thickness of 1.5 mm in a vertical rectangular mold (Fig. 1(a)). In the other case samples were cast with a thickness of approx. 130 micron (0.13 mm) in a conical stainless steel mold (Fig. 1(b)). In both cases a solid charge was first inserted into the mold and then melted in a vacuum furnace. The charges were held at a temperature above the melting point for 10 minutes, the vacuum was then released and the mold containing the molten sample was then removed from the furnace and immediately water quenched.

Figure 2 compares the temperature versus time histories of the two types of samples obtained during the quench process. The initial cooling rate of the bulk sample was approx. -7.8 ºC/sec, while the initial cooling rate of the thin cast sample was -18.7 ºC/sec. It shows that both sample types exhibited under-cooling as compared to the 217ºC equilibrium solidification temperature of Sn3.9Ag0.6Cu. The under cooling of the thin cast sample was significantly larger

than that of the bulk sample. The figure further shows that the time required for primary solidification was longer in the case of the bulk material than what was measured for the thin cast material. The reduced solidification time was likely the result of the significantly lower volume, and consequently the significantly lower latent heat produced by the thin cast charge. Following quench, all of the experimental materials were aged 4 hours at 120°C prior to creep testing.
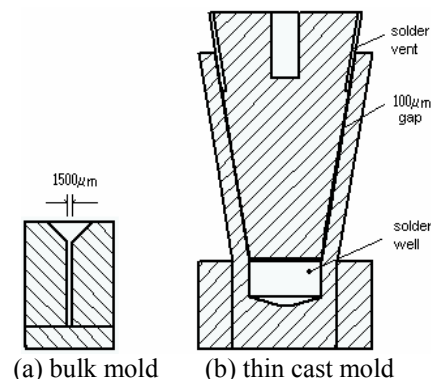

Fig. 1   Bulk and thin cast material mold designs. Molds were made of stainless steel.
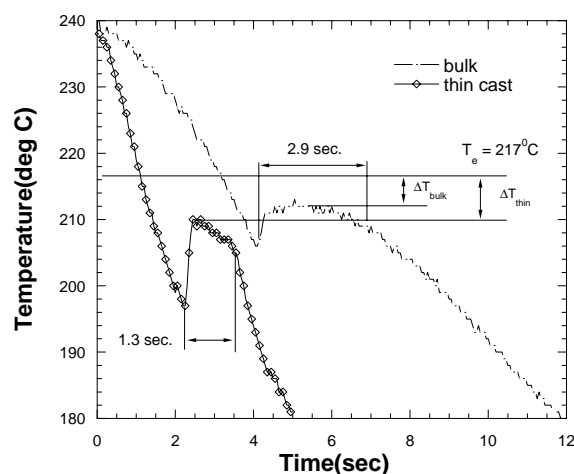

Fig. 2   Comparison of temperature versus time histories measured during water quenching for the bulk and thin cast material. Temperatures were measured by a thermocouple in contact with the solder inside the casting molds

The relatively greater under-cooling of the thin cast samples as compared to the bulk samples should be expected to result in enhanced nucleation. The relatively short primary solidification time of the thin cast material as compared to the bulk material should be expected to reduce the amount of growth of individual phases in the alloy. It is therefore reasonable to expect the thin cast material to exhibit a significantly finer microstructure than that of the bulk material. Figure 3 shows that the thin cast material does indeed show a significantly finer microstructure than that of the bulk material. The figure shows that both the bulk and thin cast microstructures consists of a mixture of eutectic regions of dispersed intermetallic compounds (IMC) which

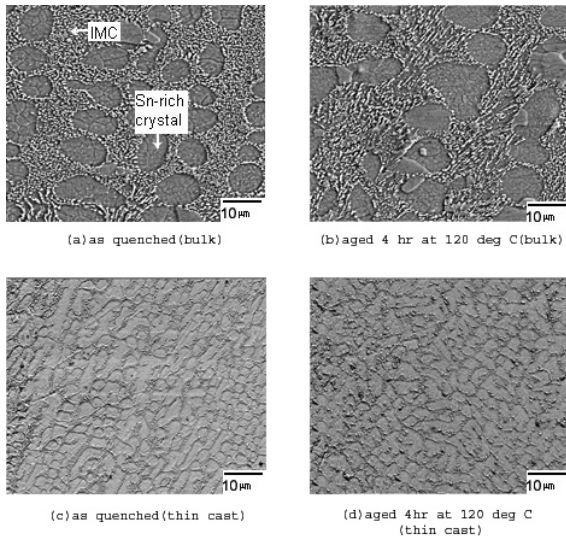surround large beta-Sn crystals (phases are identified in Fig. 3(a)).

(a) as quenched (bulk)

(b) aged 4 hr at 120 deg C (bulk)

(c) as quenched (thin cast)

(d) aged 4hr at 120 deg C (thin cast)

Fig. 3   Comparison of SEM-BSE micrographs of bulk and thin cast, as-quenched and as-aged 120^0C four hours Sn3.9Ag0.6Cu microstructures. Samples lightly etched with 2 vol% HCl in ethanol solution.

The tiny precipitates have been previously identified as the Ag_3Sn and Cu_6Sn_5 intermetallic phases [13]-[20]. In the bulk sample, the IMC eutectic forms a thick continuous network which isolates individual large size beta-Sn grains. In the thin cast sample the beta-Sn grains are small and semi-connected while the IMC eutectic form a thin semi-continuous network. A comparison of Figs 3(a) and 3(b) shows that both the beta-Sn and IMC particles coarsen in the bulk sample after aging for four hours at 120^oC . A similar comparison of Figs 3(c) and 3(d) shows that both the beta-Sn and IMC particles also coarsen in the thin cast sample after aging for four hours at 120^oC, however even after aging for four hours at 120^oC the thin cast microstructure is much finer than the bulk microstructure.

Figure 4 shows a schematic diagram of the creep test machine which was used for the thin cast material. The specimen was loaded by a dead load through a copper wire wound onto a rotary variable inductance transducer (RVIT). The specimen temperature was held constant by thermocouple controlled infrared lamps as the sample was immersed in mineral oil inside a glass container.   The sample was maintained at the test temperature 30 minutes before loading was applied, and temperatures remained constant to $\pm$ 0.2ºC during the course of testing. The tests of the thin cast Sn3.9Ag0.6Cu alloy were carried out at 45, 80, 115, and 150ºC, corresponding to the homologous temperatures (T/Tm) of 0.64, 0.72, 0.79, and 0.86 respectively.

Following creep testing, specimens were examined metallographically.   Each specimen was ground with SiC papers and then mechanically polished with diamond paste. The finest polish size was 0.25 micron. All samples were etched for a few seconds with 2 vol % hydrochloric acid in ethanol. SEM and Microprobe analyses were then performed to identify microstructures. The SEM used was a JEOL JSM

5800-LV. The microprobe machine used was a JEOL JXA-8900R (WD/ED combined microanalyzer), both with an accelerating voltage of 20keV.
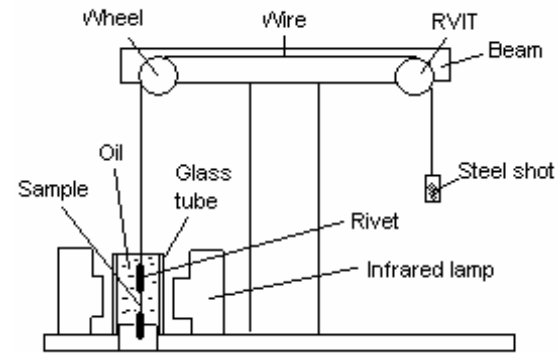

Fig. 4   Schematic diagram of the thin cast specimen creep test setup.

RESULTS AND DISCUSSION

CREEP CURVES

Figure 5(a) shows a typical example of a set of creep curves obtained at one temperature, in this case 80^0C. Figure 5(b) shows the corresponding strain rate curves obtained by time differentiation of the creep curves. Each test was continued until the minimum true strain rate was identified. Experiments which did not produce a reasonable period of stabilized minimum creep rate were not included in the final data set. The full set of steady-state creep rates of thin cast material for specified temperatures and applied stresses are listed in Table 1.

(a)

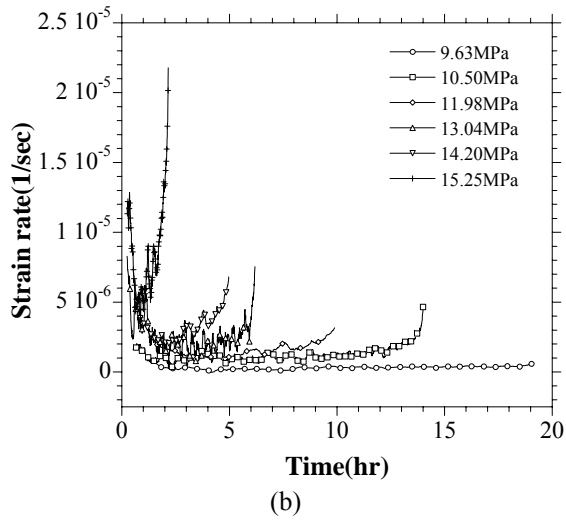Copyright © 2005 by ASME

(b)
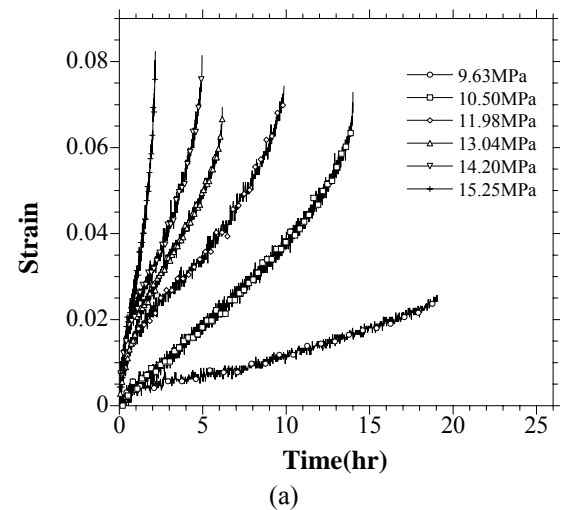
Fig. 5 An example set of creep curves from thin cast Sn3.9Ag0.6Cu samples tested at 80°C. additional data sets were collected at 45, 115 and 150°C.

Table 1. Experimentally observed minimum creep rates of thin cast Sn3.9Ag0.6Cu.

T(K)	σ(MPa)	$\dot{\varepsilon}$(1/sec)
318	10.37	3.82e-08
318	11.33	6.94e-08
318	12.29	1.35e-07
318	13.38	3.12e-07
318	14.75	1.02e-06
353	9.63	6.02e-08
353	10.50	1.04e-07
353	11.98	2.77e-07
353	13.04	6.93e-07
353	14.20	1.82e-06
388	8.53	1.68e-07
388	9.18	2.54e-07
388	10.52	5.69e-07
388	11.85	1.41e-06
388	12.65	2.51e-06
423	6.58	4.94e-07
423	7.52	7.86e-07
423	8.61	1.42e-06
423	9.48	2.52e-06
423	10.42	4.61e-06

Figure 6 shows the comparison between the full experimental creep rate data sets of the bulk and thin cast materials by plotting the quantity $\dot{\varepsilon}(T/G)$ against modulus compensated stress (σ/G) in the log-log format. The slope of the lines between two points, which provides the local value of the stress exponent, is written into the figure. In most cases five stress points were measured at each of the four test temperatures: 45, 80, 115, 150°C. The figure shows that the results follow a similar general trend. Both sets of data exhibit an increasing stress exponent with increasing stress at a fixed temperature. Both sets of data show generally converging

fixed temperature lines. In the low stress regime, n value of 6.50-6.86 was observed at 45 and 80°C, while at 115 and 150°C, n was about 4.35-5.69. At the high stress regime, there is a change in slope with a high n-value of ~7-11. Our present stress range is at or below the range investigated by Dutta et al [1]. It is difficult to directly compare our results with those of the other studies [2]-[5] since the target alloy is different (Theirs is Sn3.5Ag, ours is Sn3.9Ag0.6Cu), and the fact that their testing was performed in compression/shear while ours was performed tension.
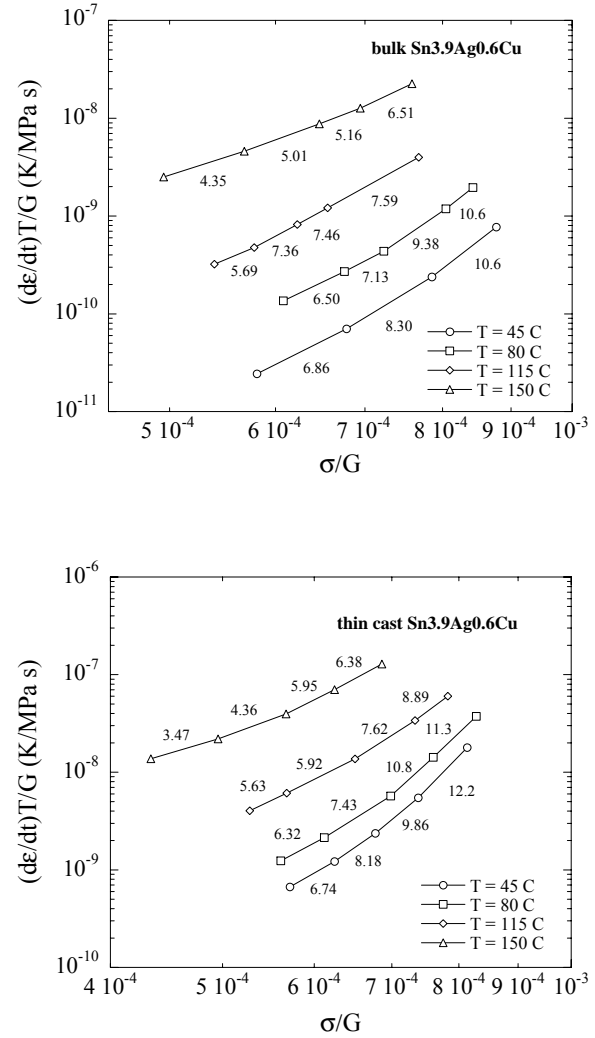

Fig. 6 Steady state creep rates of Sn3.9Ag0.6Cu plotted against applied stress at 45, 80, 115 and 150ºC. The numbers inside the plot are the local stress exponent values.

Figure 7 compares the steady-state creep rates of thin cast Sn3.9Ag0.6Cu alloy to that of bulk Sn3.9Ag0.6Cu alloy at 45 and 115ºC. Clearly, the thin cast material is less creep-resistant than the bulk. The strain rate of the thin cast material is as much as 10 times higher than that of the bulk material at the lower temperature. The slopes of the two data sets are similar indicating similar values of stress exponent, and therefore similar dominate creep mechanisms.
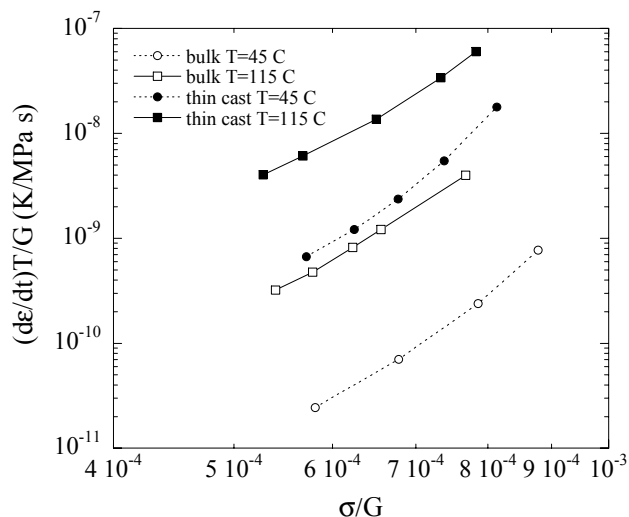
Fig. 7   Comparison between the creep behaviors of bulk and thin cast Sn3.9Ag0.6Cu at temperatures of 45 and 115ºC.

METALLOGRAPHY OF SN-3.9AG-0.6CU ALLOY

Figures 8 and 9 compare back scatter electron images and Sn, Ag and Cu element maps for bulk and thin cast samples after being crept under similar stress levels at 115°C. Figure 8 shows the microstructure of bulk and thin cast samples after aging at 120°C for four hours. The BSE (back scattered electron) image indicated microstructures agree well with that shown earlier in Figs. 3(b) and 3(d). The Ag and Cu maps show very important differences in the IMC eutectic structure exist between the bulk and thin cast materials. The bulk material exhibits a fine grained IMC eutectic that well separates the beta-Sn grains, while the IMC eutectic in the thin cast materials is in the form of a thin network. A comparison of Cu maps indicates greater coarsening in the as-aged thin cast sample. Clearly, both the bulk and thin cast microstructures evolve during creep. A comparison between the Ag maps of Figs 8 and Figs 9 shows that the IMC eutectic structure of the bulk cast material remains relatively intact after creep with numerous coarse Ag$_3$Sn decorating beta-Sn grains, while the thin IMC eutectic network of the as-aged thin cast sample suffers severe break up and coarsening. In fact, the IMC structure of the as-crept 115°C thin cast material appears to be reduced to that of isolated coarse particles separated by continuous beta-Sn.
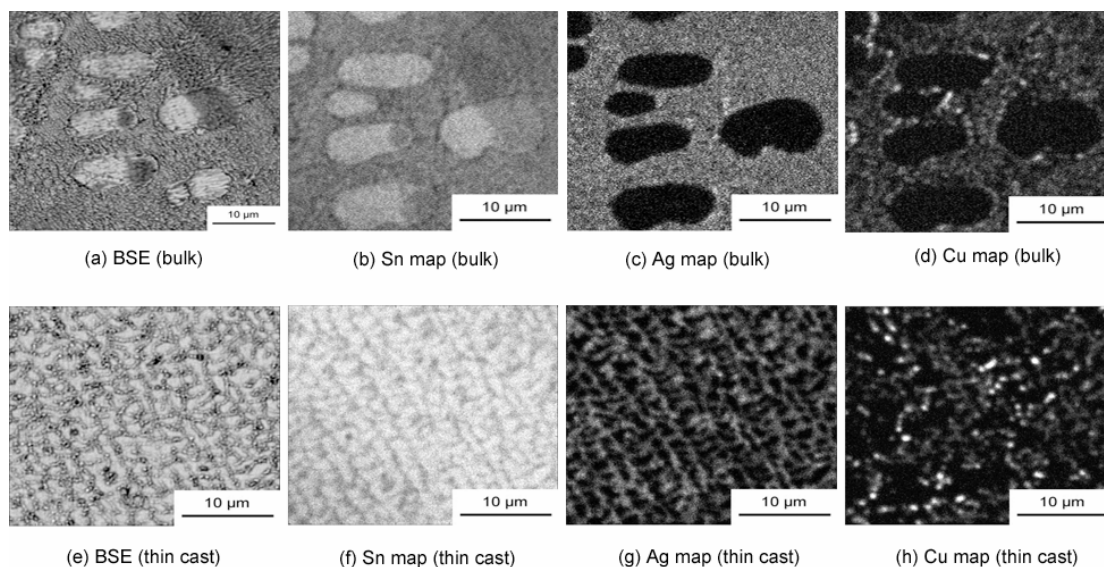

(a) BSE (bulk)   (b) Sn map (bulk)   (c) Ag map (bulk)   (d) Cu map (bulk)

(e) BSE (thin cast)   (f) Sn map (thin cast)   (g) Ag map (thin cast)   (h) Cu map (thin cast)

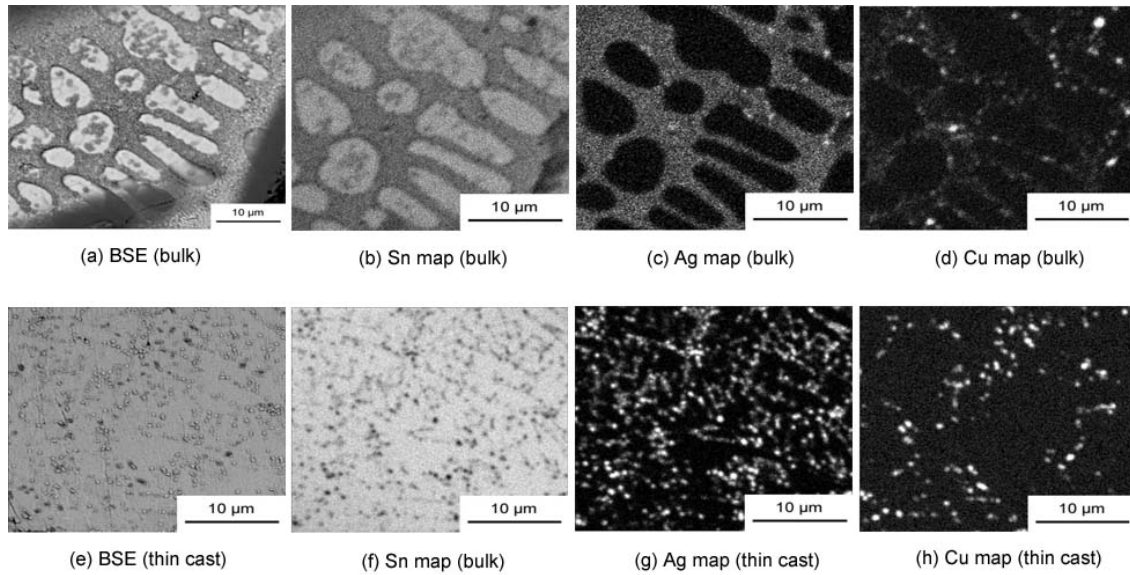Fig. 8   Comparison of as-aged 120 C for four hours bulk and thin cast Sn3.9Ag0.6Cu microstructures.

Fig. 9   Comparison of (a-d) bulk and (e-h) thin cast Sn3.9Ag0.6Cu microstructures, samples were first aged four hours at 120^0C then crept at 115ºC under applied stress of 10.6 and 10.5 MPa.

CONSTITUTIVE MODELING AND ANALYSIS

Figure 10 compares the effect of temperature on the steady state creep rates of bulk and thin cast material by plotting $\ln(\dot{\varepsilon}\,T/G)$ against (1/T). The slopes of the curves represent an estimation of the average activation energy, $Q_c = -R\dfrac{d(\ln \dot{\varepsilon}T/G)}{d(1/T)}$ (where R is the gas constant). Figure 10(a) compares data measured at σ =10.4-10.5 MPa, and Fig. 10(b) compares data measured at σ =12.0-12.4 MPa. In both cases the average activation energies of the bulk material are larger than that of the thin cast material.

Figure 11 shows the best fit between the experimental data and the Dorn power law constitutive model given by,

$$\dot{\varepsilon} = A\sigma^n \exp\left(-\frac{Q}{RT}\right) \qquad (1)$$

where T is the absolute temperature, R is the gas constant, n is the stress exponent, and Q is the activation energy. Table 2 shows the fit values of n and Q. The figure and table shows that the value of the model stress exponent is nearly the same between the bulk and thin cast material. However, the model activation energy for the bulk material is larger than that for the thin cast material.
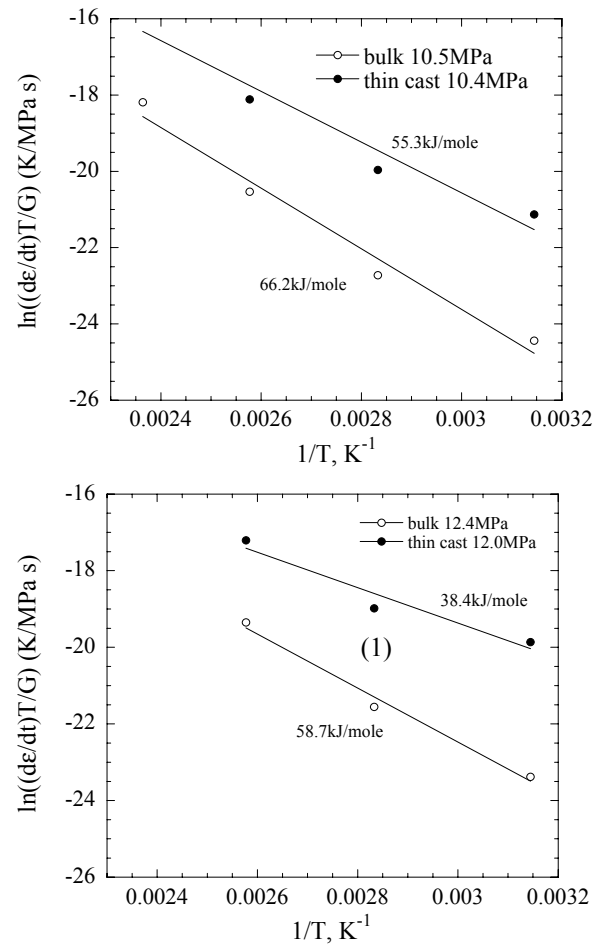

Fig. 10   Comparison between bulk and thin cast Sn3.9Ag0.6Cu activation energies under stresses of (a) 10.4-10.5 MPa and (b) 12.0-12.4 MPa.

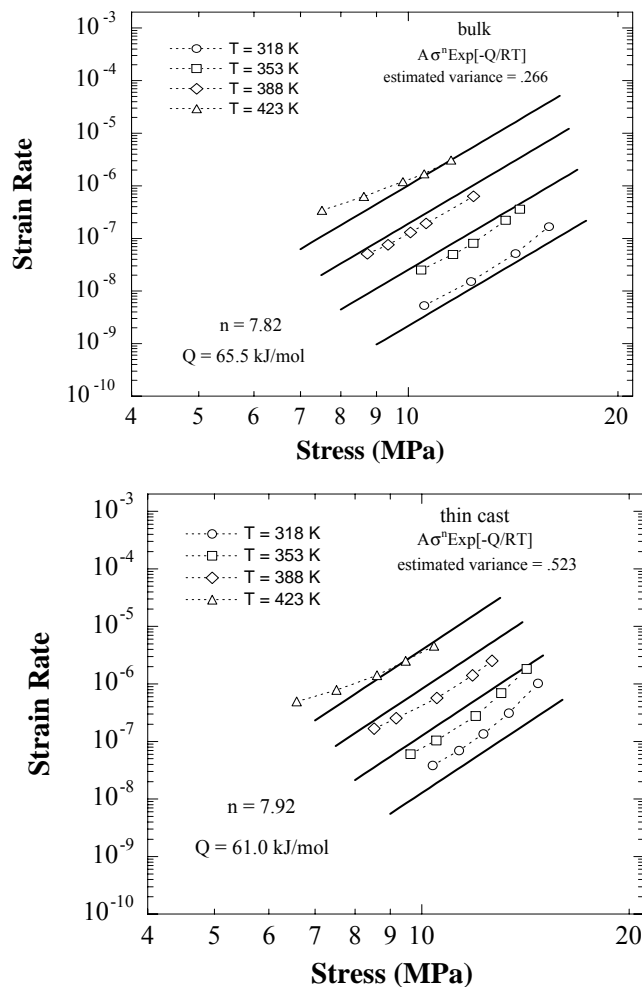6   Copyright © 2005 by ASME

Fig. 11 Comparison between Dorn model and experimental creep strain rates of (a) bulk and (b) thin cast Sn3.9Ag0.6Cu. Figures include the stress exponent, n, activation energy, Q, and estimated variance obtained by model fitting.

Table 2. Dorn model best fit parameters

sample	n	Q(kJ/mol)
bulk	7.82	65.5
thin cast	7.92	61.0

Figure 12 shows the best fit between the experimental results and the well known Garofalo model [21]-[22]. The model is given by,

$$\dot{\varepsilon} = c_1 \sinh[c_2\sigma]^{c_3} \exp\left(-\frac{Q}{RT}\right) \qquad (2)$$

where again R is the gas constant, and Q is the activation energy. Table 3 provides the parameters of the Garofalo model. The analysis again indicates that the activation energy

for the bulk material is significantly higher than that for the thin cast material.
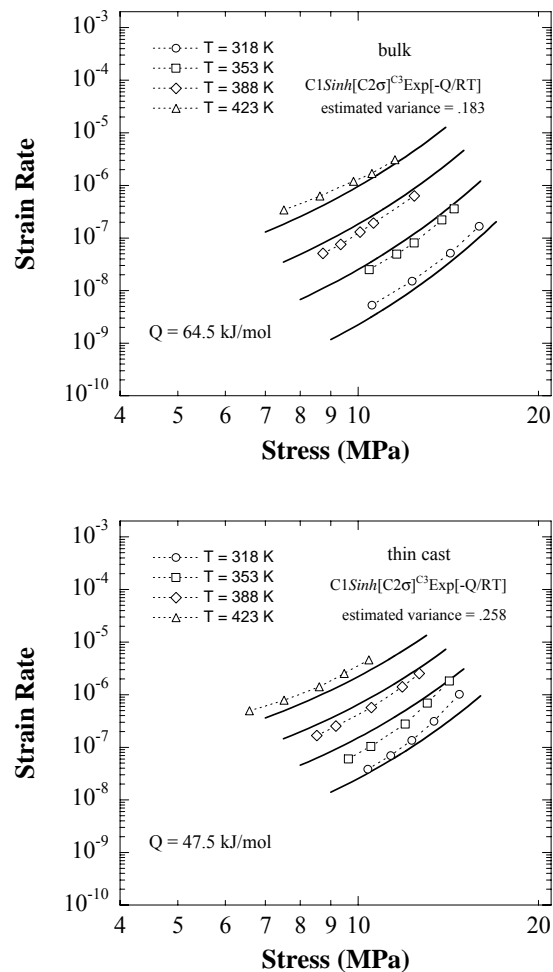

Fig. 12   Comparison between Garofalo model and experiment creep strain rates of (a) bulk and (b) thin cast Sn3.9Ag0.6Cu. Figures include the stress exponent, n, activation energy, Q, and estimated variance obtained by model fitting.

Table 3. Garofalo model best fit parameters

Sample	C1(1/sec)	C2	C3	Q(kJ/mol)
bulk	1.05	0.229	2.80	64.5
thin cast	0.006	0.951	0.633	47.5

In each of the experimental cases for both alloys the temperature was high enough to indicate creep thermal activation as a dominate rate controlling mechanism. Figure 13 represents the energy relationships for this process [23]. Here a positive deformation event occurs when a local region transitions from state A to state B. The local state must pass over an energy barrier of magnitude q in order to accomplish this transition. The application of a stress effectively lowers the potential energy of state B and raises the potential energy of state A by an amount w. The frequency of the transition

from A to B, $v_{A->B}$, and the frequency of the transition from B to A, $v_{B->A}$ are then given by,

$$v_{A->B} = v_0 \exp\left(-\frac{q-w}{kT}\right)$$
$$v_{B->A} = v_0 \exp\left(-\frac{q+w}{kT}\right)$$

(3)

where T is the temperature in Kelvin, k is Boltzman's constant, and v_0 is a scaling factor. Each transition event results in a small increment of strain. Therefore the strain rate is given by

$$\dot{\varepsilon} = A(v_{A->B} - v_{B->A}) = A v_0 \left(\exp\left(-\frac{q-w}{kT}\right) - v_0 \exp\left(-\frac{q+w}{kT}\right)\right)$$

(4)

where A is a nondimensional constant. Equation 4 may be rewritten in a compact form by applying the definition of the hyperbolic sine function,

$$\dot{\varepsilon} = A\left[\sinh\left(\frac{w}{kT}\right)\right]\exp\left(-\frac{q}{kT}\right)$$

(5)

The energy difference due to the presence of stress, w, may be expected to depend on the magnitude of the stress. In the present study we assume that the dependence has a general power law form,

$$w = \alpha\tau^{\beta}$$

(6)

where τ is the shear stress, and α and β are constants. Equation 5 may then be rewritten in an experimentally useful form assuming the solder obeys the von Mises criterion,

$$\dot{\varepsilon} = c_1\left[\sinh\left(\frac{c_2\sigma^{c3}}{RT}\right)\right]\exp\left(-\frac{Q}{RT}\right)$$

(7)

where R is the gas constant, and Q is the activation energy. We will refer to this model as the power-law-stress-dependant-energy-barrier-model.
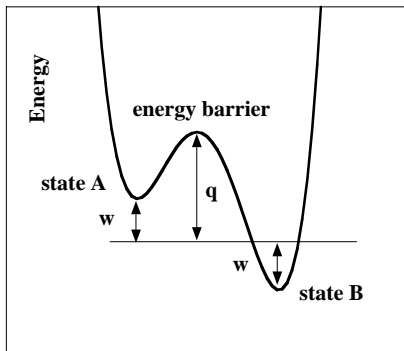

Fig. 13   Representation of the energy relationships for the thermally activated creep process.

A positive deformation event occurs when a local region transitions from state A to state B. The local state must pass over an energy barrier of magnitude q in order to accomplish this transition, see figure 13. Figure 14 shows the best fit between the experimental results and the power-law-stress-dependant-energy-barrier model.   Table 4 provides the

corresponding best fit parameters of the model. The analysis again indicates that the activation energy for the bulk material is significantly higher than that for the thin cast material. A comparison of Figs. 11, 12, and 14 shows that the estimated variances returned by the fitting procedure is lower when using the power-law-stress-dependant-energy-barrier model than when using the Garofalo model, and that the estimated variances returned by the fitting procedure is lower when using the Garofalo model than when using the Dorn model. This indicates that the power-law-stress-dependant-energy-barrier model provides the best fit to the present experimental data.
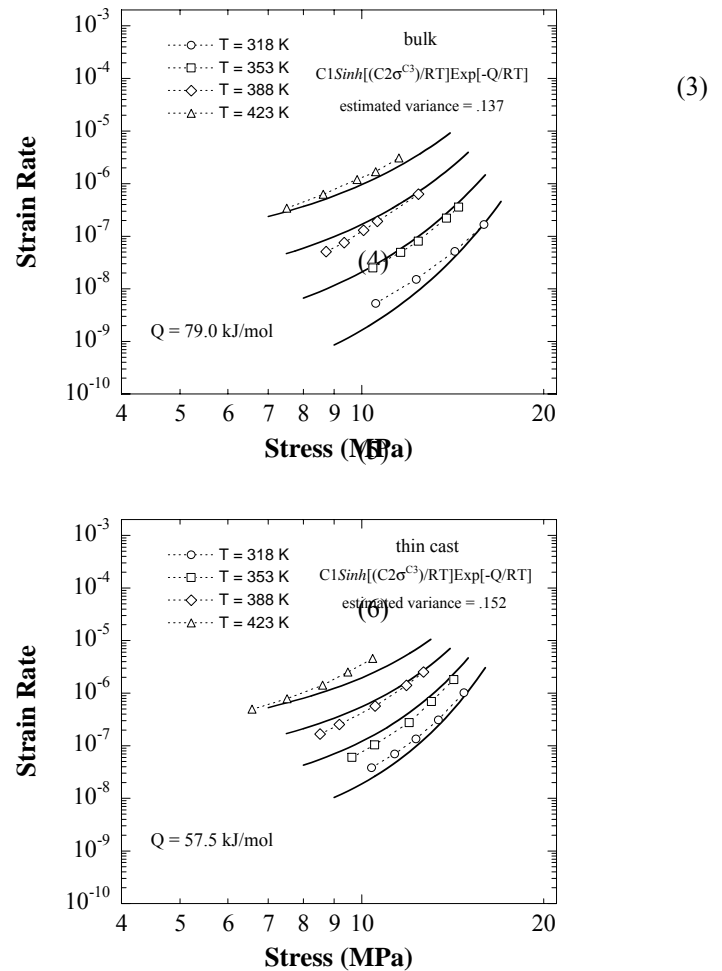

Fig. 14   Comparison between power-law-stress-dependant-energy-barrier model and experimental creep strain rates of (a) bulk and (b) thin cast Sn3.9Ag0.6Cu. Figures include the stress exponent, n, activation energy, Q, and estimated variance obtained by model fitting.

Table 4. Power law stress dependant energy barrier model best fit parameters.

Sample	C1(1/sec)	C2	C3	Q(kJ/mol)
bulk	467.4	275.3	1.61	79.0
thin cast	5.26	61.5	2.11	57.5

A second consideration of the electron microscopy results shown in Figs. 8-12 provides an explanation for the difference in the activation energies of the bulk and thin cast

materials. It is well accepted that the thick IMC eutectic provides the primary creep resistance in bulk Sn3.9Ag0.6Cu [26]-[27] through the mechanism of dispersion hardening. The value of the stress exponent indicates that the primary creep mechanism operating at the temperatures investigated in this study was climb assisted dislocation glide. A comparison of Ag element maps between as crept bulk and thin cast material shows that the relevant climb process occurs in a very different environment in the bulk material as compared to the thin cast material. In the bulk material the relevant climb process occurs within a finely dispersed IMC eutectic which covers broad areas within the material. In the thin cast material the relevant climb process occurs primarily in the beta-Sn grains which continuously surround isolated, coarse IMC particles. The internal stress within the bulk material eutectic beta Sn is likely to be much higher and therefore more likely to impede dislocation glide and climb, clearly the degree of dispersion hardening should be significantly higher in the bulk material eutectic beta-Sn. It therefore seems reasonable that the observed strong differences in as-crept IMC microstructures would result in measurable differences in activation energy.

MODELING AND MEASUREMENT OF HEAT STRESSING OF MICRO-SMD ASSEMBLY

The thermal-mechanical response of electronic packages was simulated using the commercial finite element code ANSYS coupled with the Garofalo model to represent the solder constitutive creep response. Measured properties shown above for bulk and thin-cast Sn3.9Ag0.6Cu SAC alloy were used. Building finite element models of electronic assemblies requires details of the package configuration and the layout and geometry of the solder interconnects. Simulations of thermal cycling, in turn, require accurate material properties. For most packaging materials, the mechanical material properties are available in the published literature [26]-[27]. However, the constitutive modeling of the SAC alloy requires direct measurement. The test vehicle for this study was the 3 mm by 3 mm NSC Thin Micro-SMD 36 bump 0.5 mm pitch chip-scale package. The layout of the I/O for this package is shown below in Figure 15.
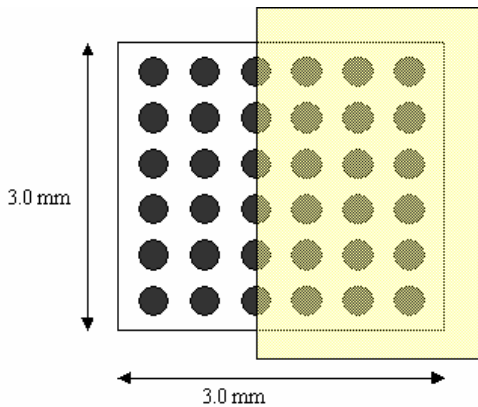

Fig. 15 Layout of the 36 I/O Micro-SMD bump pattern.

The shaded region of the package in Figure 15 indicates the part modeled in ANSYS. This was due to the cross-sectioning

done during sample preparation for moiré testing. Other package details are shown in Table 5.

Table 5. 36 I/O Micro-SMD Package Dimensions

Parameter	Dimension
Die thickness	330 μm
Solder Joint Height	216 μm
Solder Joint Diameter	430 μm
Board thickness	62 mils
Pitch	0.5 mm

To reduce the computational overhead, symmetry conditions present in the package were invoked. As shown in Figure 15, the shaded region represents the portion of the package remaining after sample preparation for moiré testing. The lightly cross-hatched region is the portion that was modeled, thereby invoking symmetry as shown in figure 16. In ANSYS, appropriate symmetry boundary conditions were applied
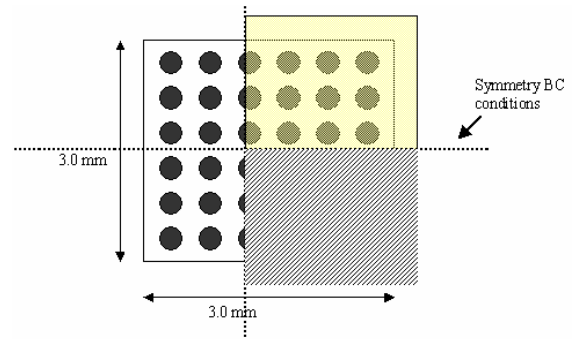

Fig. 16 Layout of the 36 I/O Micro-SMD showing symmetry.

The ANSYS finite element model for this package was composed of 18,000 elements. Those elements comprising the solder joints were modeled with ANSYS element Solid 185, which is a 3-D element capable of creep response. The rest of the package and board were modeled with ANSYS 3-D element Solid 45. Figure 17 shows a view of the finite element model of the package showing the solder joints. The joints that are "cut" along their face represent the joints cross-sectioned for moiré testing. A close-up of a typical solder joint mesh is shown in Figure 18.
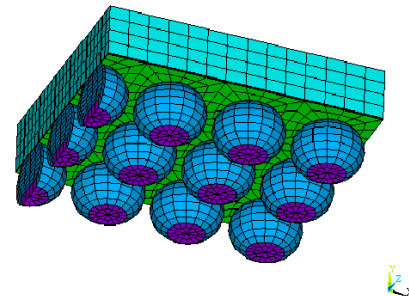

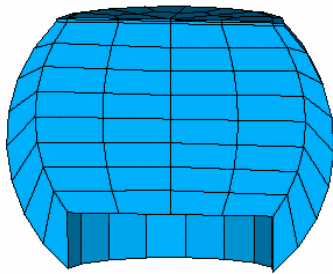Fig. 17 Finite element mesh of the 36 I/O Micro-SMD package.

Fig. 18 Finite element mesh of a typical solder joint along the cross-section.

Free-edge boundary conditions were assumed, consistent with the test fixture used in for the moiré measurements. Material properties for the model were taken from the published literature and from previous work by the authors. Table 6 summarizes the properties used in the model. The Garofalo creep equation, described above, was used for the Sn3.9-Ag0.6-Cu alloy.

Table6. Constants for Garofalo Constitutive Model in ANSYS

Sn 3.9-Ag 0.6-Cu Sample Type	A (1/sec)	B (1/Mpa)	C	D (K)
Bulk	0.184	0.221	2.89	7,484.6
Thin-cast	0.006	0.951	0.633	5,734.2

MOIRE TECHNIQUE

Moiré interferometry is a technique that utilizes several different optical principles to measure the in-plane displacement of a sample due to a load. The optical principles that the moiré interferometer is based upon are the moiré effect, interferometry and diffraction. The results of a moiré analysis are full-field in-plane displacements in the form of a fringe pattern. The equations that govern the relationship between fringe order and in-plane displacement are expressed as:

$$U = \frac{1}{f} N_x$$
$$V = \frac{1}{f} N_y$$
(8)

Here U and V are the in-plane displacement fields in the x- and y-directions, respectively, and N_x and N_y are their respective fringe orders. The quantity f is the frequency of the reference grating. Using moiré interferometry, in-plane displacements can be measured with an accuracy of 0.417 µm per fringe order [28]. This system provides accurate measurements of the in-plane displacements via the use of post-processing software. In addition, we have developed post-processing software to further enhance our data analysis capabilities with fringe-shifting techniques.

Moiré interferometry requires a flat surface on which a grating can be replicated. Depending on the information needed, the sample is cross-sectioned and ground flat on the plane of interest. The grinding ensures that a flat, clean surface is available for adhesion of the cross-lined grating. The cross-lined grating used for replication is typically mounted on an ultra-low expansion (ULE) glass substrate, to ensure that the effect of the thermal load on the reference grating is very small. The gratings are produced with a frequency of 1,200 lines/mm along two orthogonal axes. The diffraction efficiency of the grating is optimized for use in moiré interferometry [29].

The prepared sample and the grating mounted on a ULE glass substrate are pre-heated in an oven to 100ºC. The sample and grating are then removed from the oven. A thin, even layer of high temperature, low viscosity epoxy is applied to the surface of the sample using an optical grade (i.e., lintless) tissue. The sample is then pressed onto the grating, and placed back into the oven to cure the epoxy. Care must be taken to ensure that the sample is not out of the oven for an extended period. Once the sample has cured, it is removed from the oven and the ULE grating is immediately removed. The sample then cools to room temperature and is subsequently ready for moiré analysis. The measured cool down curve for the SAC alloy assemblies is shown in Figure 19.
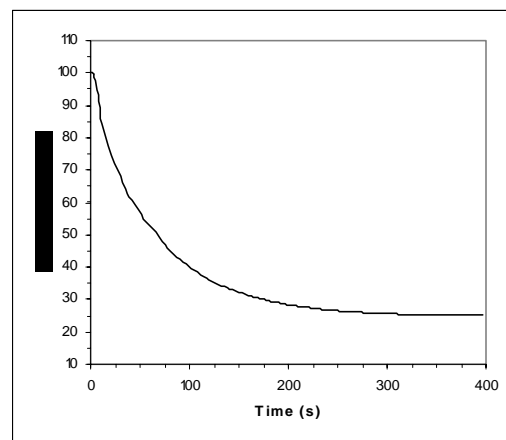

Fig. 19 Measured cooling curve of assembled SAC Alloy Sample

Once the assembly was cooled, it was placed into the interferometer. After setup and calibration, the optical fringe patterns of the assembly were captured using a digital camera. A typical optical fringe pattern is shown in Figure 20.

Fig. 20 Optical fringe image for horizontal displacement of the SAC alloy sample.

Using fringe-shifting techniques, a series of fringe images are recorded and then processed with the use of the computer. Note that this post-processing does not improve the fundamental resolution of the system, but rather, it helps

define fractional fringe orders. The image shown in Figure 21 has been processed by this method. The contour lines of horizontal displacement are spaced at 100.7 nm.
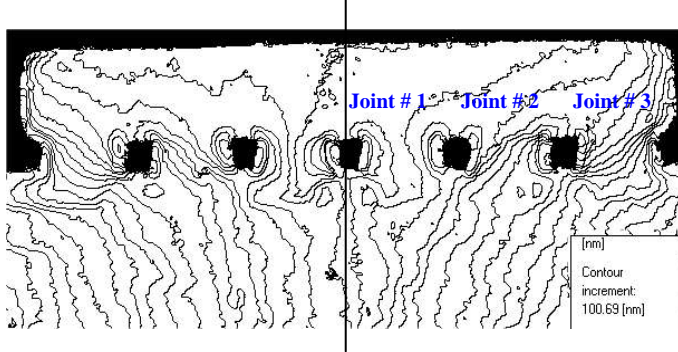

Fig. 21 Computer-enhanced fractional fringe image for horizontal displacement for the SAC alloy sample.

Using the computer model to simulate the cool down from 100°C to room temperature (using the measured cool down curve shown in Figure 19), the resulting relative horizontal displacement between top and bottom of the end-row solder joints was computed. For these packages, the horizontal displacement typically dominates the response and is a leading contributor to fatigue damage in the solder joint. This displacement is compared to that measured from the moiré technique. Data from ten samples was averaged to produce the measured results reported below.

As can be seen in Table 7, both the bulk and thin-cast models predictions had mixed agreement in the three solder joints. The joint # 1 is close to the center and is expected to have the least displacement. In the case of the joint # 2, the predictions are better using thin cast model compared to the bulk properties. The end joint measured displacement is close the value predicted using bulk properties. It is noted that the assemblies used the Sn3.8Ag0.6Cu alloy while the creep model assumed the Sn3.9Ag0.6Cu alloy. It is not known if this difference could cause any change in the results.

Table 7. Comparison of measured and predicted displacement in the end-row solder joint.

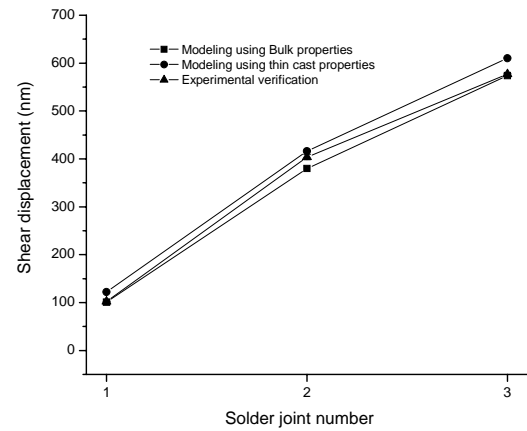| Joint #	Average Measured value (nm)	Modeling	
		Bulk Properties	Thin cast properties
1	102	101	122
2	404	380	416
3	577	574	610

Fig. 22 Comparison of displacements in the three joints between experiments and predictions.

SUMMARY AND CONCLUSIONS

The present paper compares the creep and microstructural changes during creep behaviors of bulk and thin cast forms of Sn3.9Ag0.6Cu. The processing parameters of the thin cast material were selected to result in a very fine microstructure analogous to what occurs in very small size solder electronic interconnections.

This work supports the following conclusions:

(1). The thin cast material is less creep-resistant than the bulk material. The strain rate of the thin cast material is as much as 10 times higher than that of the bulk material at the lower test temperatures.

(2). Very important differences in the IMC eutectic structure exist between the bulk and thin cast materials. The bulk material exhibits a fine grained IMC eutectic that well separates the beta-Sn grains, while the IMC eutectic in the thin cast materials is in the form of a thin network. The IMC eutectic structure of the bulk cast material remains relatively intact after creep, while the thin IMC eutectic network of the as-aged thin cast sample suffers severe break up and coarsening.

(3). The value of the stress exponent is nearly the same between the bulk and thin cast material. However, the activation energy of the bulk material is larger than that for the thin cast material. A comparison of Ag element maps between as crept bulk and thin cast material shows that the relevant climb process occurs in a very different environment in the bulk material as compared to the thin cast material. In the bulk material the relevant climb process occurs within a finely dispersed IMC eutectic which covers broad areas within the material. In the thin cast material the relevant climb process occurs primarily in the beta-Sn grains which continuously surround isolated, coarse IMC particles. It therefore seems reasonable that the observed strong differences in as-crept IMC microstructures would result in measurable differences in activation energy.

(4). Finally, it is important to note that the strength deficiency of the thin cast material is persistent, once the material is cast in thin cast form it will remain weak in comparison to the bulk

11   Copyright © 2005 by ASME

material. Therefore, using data obtained from bulk material samples for the construction of thermomechanical models of very small scale solder interconnections is likely to result in significant, intrinsic errors.

(5). It has been shown that the thermal-mechanical response of actual electronic packages can be simulated using the commercial finite element code ANSYS. The approach used the Garofalo model to represent the solder constitutive creep response with measured properties for the Sn3.9Ag0.6Cu SAC alloy. The model produced good correlation with the horizontal solder joint displacement measurement using both bulk as well as thin case properties. The assemblies tested used the Sn3.8Ag0.6Cu alloy rather than the Sn3.9Ag0.6Cu alloy. It is not known if this difference is significant to the thermo-mechanical response.

REFERENCES

1. I. Dutta, "A Constitutive Model for Creep of Lead-Free Solders Undergoing In-situ Microstructural Coarsening: A First Report", J. Electron. Mater., 2003, pp. 201-207.

2. R.A. Marks, et al., "Constitutive Model for Creep of Lead-Free Solders Undergoing In-situ Microstructural Coarsening", 9th Intersociety Conference on Thermal and Thermomechanical Phenomena, 2004, pp.95-102.

3. H.G. Song, et al., "Anomalous Creep in Sn-Rich Solder Joints", Trans. JIM, ,2002, pp. 1847-1852.

4. H.G. Song, et al, "The Creep Properties of Lead-Free Solder Joints", J. Metals, 2002, pp. 30-32.

5. F. Hua, "Pb-free Solder Challenges in Electronic Packaging and Assembly", 53rd Electron. Comp. Technol. Conf., 2003, pp. 58-63.

6. F. Garofalo, "A Empirical Relation Defining the Stress Dependence of Minimum Creep Rate in Metals",Trans. AIME, 1963, pp. 351-365.

7. John. Lau, et al., "Acceleration models, constitutive equations, and reliability of lead-free solders and joints", 53rd Electron. Comp. Technol. Conf., 2002, pp. 229-236.

8. John H.L. Pang, et al., "Creep and Fatigue Characterization of Lead Free 95.5Sn-3.8Ag-0.7Cu Solder",54th Electron. Comp. Technol. Conf., 2004, pp. 1333-1337.

9. A. Schubert, et.al., "Reliability Assessment of Flip-Chip Assemblies with Lead-free Solder Joints", 53rd Electron. Comp. Technol. Conf., 2003, pp. 603-610.

10. Q. Zhang, et al., "Viscoplastic constitutive properties and energy-partitioning model of lead-free Sn3.9Ag0.6Cu solder alloy", 53rd Electron. Comp. Technol. Conf., 2003, pp. 1862-1868.

11. S. Wiese, et al., "Microstructural dependence of constitutive properties of eutectic SnAg and SnAgCu solders", 53rd Electron. Comp. Technol. Conf., 2003, pp. 197-206.

12. Q. Xiao, et al., "Aging and Creep Behavior of Sn3.9Ag0.6Cu Solder Alloy"54th Electron. Comp. Technol. Conf., 2004, pp. 1325-1332.

13. Q. Xiao, et al., "Tensile Creep and Microstructural Characterization of Bulk Sn3.9Ag0.6Cu Lead-Free Solder", J. Electron. Mater. 2005, pp. 196-211.

14. Q. Xiao, L. Nguyen, and W. D. Armstrong, "The Anomalous Microstructural, Tensile and Aging Response of Thin Cast Sn3.9Ag0.6Cu Lead Free Solder", J. Electron. Mater. in press.

15. Q. Xiao, H. J. Bailey, and W. D. Armstrong, "Aging Effects on Microstructure and Tensile Property of Sn3.9Ag0.6Cu Solder Alloy", J. Elect. Pack. 2004, pp. 208-212.

16. K. W. Moon, et al., "Experimental and Thermodynamic Assessment of Sn-Ag-Cu Solder Alloys", J. Elect. Mat. 2000, pp. 1122-1136.

17. I. Ohnuma, et al., "Phase Equilibria and the Related Properties of Sn-Ag-Cu Based Pb-Free Solder Alloys", J. Elect. Mat. 2000, pp. 1137-1144.

18. I.E. Anderson, et al., "Alloying Effects in Near-Eutectic Sn-Ag-Cu Solder Alloys for Improved Microstructural Stability", J. Electron. Mater. 2001, pp. 1050-1059.

19. D. Lewis, et al., "Determination of the Eutectic Structure in the Ag-Cu-Sn System", J. Electron. Mater. 2002, pp. 161-167.

20. John H.L. Pang, et al., "Bulk solder and solder joint properties for lead free 95.5Sn-3.8Ag-0.7Cu solder alloy", 53rd Electron. Comp. Technol. Conf., 2003, pp. 673-679.

21. J.J. Stephens, et al., "Time-Dependent Deformation Behavior of Near-Eutectic 60Sn-40Pb Solder", Metall. Mater. Trans. A, 1999, pp. 1301-1313.

22. F.A. Garofalo, *Fundamentals of Creep and Creep-Rupture in Metals*, (New York; MacMillian, 1965).

23. R. E. Reed-Hill and R. Abbaschian, *Physical Metallurgy Principles, 3rd ed*. (Boston: PWS Publishing Company, 1994).

24. S.K. Kang, et al., "Ag3Sn Plate Formation in the Solidification of Near-Ternary Eutectic Sn-Ag-Cu", JOM, 2003, pp. 61-65.

25. K.S. Kim, et al., "Effects of Cooling Speed on Microstructure and Tensile Properties of Sn-Ag-Cu Alloys", Materials Science and Engineering A333, 1999, pp.106-114.

26. Pitarresi, J., et al., "A parametric predictive solder joint reliability model for wafer level chip scale package," ECTC, San Diego, CA, pp. 1323-1328, 2002.

27. Darveaux, R. "Effect of Simulation Methodology on Solder Joint Crack Growth Correlation," ECTC, Las Vegas, NV, pp. 1048-1063, 2000.

28. Post, D., Han, B., Ifju, P., High Sensitivity Moiré, Springer-Verlag, New York, 1994.

29. Rayner, J. and Pitarresi, J.M., "Sample Preparation for Moiré Interferometry," *Soc. Exp. Mech*., Cincinnati, OH, June 1999, pp. 11-14.